

## LES Analysis of the Aerodynamic Surface Properties for Turbulent Flows over Building Arrays with Various Geometries

HIROMASA NAKAYAMA

*Japan Atomic Energy Agency, Ibaraki, Japan*

TETSUYA TAKEMI

*Disaster Prevention Research Institute, Kyoto University, Kyoto, Japan*

HARUYASU NAGAI

*Japan Atomic Energy Agency, Ibaraki, Japan*

(Manuscript received 27 May 2010, in final form 21 February 2011)

### ABSTRACT

This paper describes aerodynamic roughness properties for turbulent flows over various building arrays that represent realistic urban surface geometries. First, building morphological characteristics such as roughness density  $\lambda_f$  and building height variability  $V_h$ , defined respectively as the ratio of total frontal area of roughness elements to the total surface area and the ratio of standard deviation in building height to the average building height of the study site, were investigated. Next, large-eddy simulations (LESs) of turbulent flows over building arrays were performed with various surface geometries characterized by a wide range of values for both  $\lambda_f$  and  $V_h$ , based on this building morphological analysis. Third, aerodynamic roughness parameters such as roughness length  $z_0$  and drag coefficient  $C_d$  were evaluated for the central Tokyo area from the values of  $\lambda_f$  and  $V_h$  using the LES results. The values of  $z_0$  and  $\overline{C_d}$  as a function of both  $\lambda_f$  and  $V_h$  were comparable to those found in earlier studies. The values of  $z_0$  and  $\overline{C_d}$  evaluated by a conventional method using only  $\lambda_f$  were underestimated, particularly for densely built-up areas. This indicates that the present approach to estimating aerodynamic roughness parameters, taking account of both roughness density and building height variability, is more appropriate than conventional approaches when applied to actual urban areas. The roughness aerodynamic parameters as a function of  $\lambda_f$  and  $V_h$  obtained from the LES results will be useful in incorporating urban effects into weather forecasting models.

### 1. Introduction

Urbanization has produced drastic changes in land surface characteristics. Cities have become more densely built, and naturally green surfaces have been replaced with asphalt and concrete. Increased surface roughness due to artificial structures leads to a reduction in wind speeds and an increase in air temperature within the urban canopy. In particular, temperature increases in urban areas relative to their surroundings create the phenomenon known as urban heat islands; this is now an

important research topic in urban meteorology and climatology, as well as a critical environmental and social issue. Recent societal issues in urban weather and climate not only concern the viewpoint of the atmospheric environment but also extend to disaster prevention or mitigation and social safety and security. In this way, urbanization has a significant impact on local atmospheric environments that form urban weather and climate.

Numerical simulations with the use of mesoscale meteorological models are a useful and important approach when investigating the characteristics of urban weather and climate. Since atmospheric phenomena over land are strongly influenced by surface properties and processes, the geometric properties and physical processes of land surfaces should somehow be incorporated into

Corresponding author address: Hiromasa Nakayama, Japan Atomic Energy Agency, 2-4 Shirakatashirane, Tokai-mura, Naka-gun, Ibaraki 319-1195, Japan.  
E-mail: nakayama.hiromasa@jaea.go.jp

numerical models. Urban surfaces are regarded as the most complex type of land characteristic category. In mesoscale meteorological models, there are typically two approaches to representing the aerodynamic effects of urban surfaces: one based on roughness length and the other on drag force.

In the roughness-length approach, wind velocity and turbulent fluxes at the ground surface are calculated by using roughness parameters such as roughness length  $z_0$  and displacement height  $d$  based on the assumption of Monin–Obukhov similarity theory (see Fig. 1a). Roughness lengths and displacement heights can be evaluated as functions of a land-use category. Grimmond and Oke (1999) evaluated such aerodynamic parameters for a wide variety of urban areas characterized by various types of surface forms. Their findings suggest that aerodynamic properties depend significantly on the configuration of buildings and structures in cities. From a theoretical viewpoint, Macdonald et al. (1998) investigated the variation in roughness length and displacement height in airflows over regular arrays of cubic obstacles with various roughness densities and arrangements, and proposed a theoretical model for estimating roughness parameters.

The roughness approach has the advantage of easily incorporating the effects of the ground surface into mesoscale meteorological models, since it does not require an explicit representation of buildings and structures. The simplicity of this approach, however, sacrifices the realistic representation of atmospheric phenomena in urban areas. In addition, it is pointed out that this approach cannot reproduce the roughness sublayer over urban surfaces from a comparison with field measurements (Martilli et al. 2002). Furthermore, Cheng and Castro (2002) pointed out that log-law regions may not exist over extremely rough ground surfaces. Because roughness length is normally defined by identifying a logarithmic profile of mean winds, these previous studies strongly suggest that it is fundamentally difficult to estimate roughness parameters, particularly for urban cases with very randomly distributed and complex-shaped surface forms.

In the drag-force approach, meanwhile, groups of roughness elements are treated as porous media and the effects of unresolved obstacles on airflow are incorporated as a drag force in fluid dynamics equations (see Fig. 1b). Originally, Sorbjan and Uliasz (1982) conducted a numerical simulation of urban flow by incorporating drag and turbulence production within the urban canopy directly into fluid dynamics equations. In general, the momentum equations for incompressible atmospheric flows over urban roughness obstacles with the use of a drag approach are written as follow:

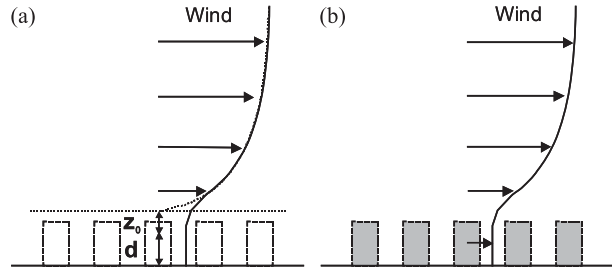


FIG. 1. The concept of incorporation of urban effects by the (a) roughness-length and (b) drag-force approaches.

$$\frac{DU}{Dt} = -\frac{1}{\rho} \frac{\partial P}{\partial x} - \frac{\partial \langle uu_j \rangle}{\partial x_j} - C_d a(z) U |U| \quad \text{and} \quad (1)$$

$$\frac{DV}{Dt} = -\frac{1}{\rho} \frac{\partial P}{\partial y} - \frac{\partial \langle vu_j \rangle}{\partial x_j} - C_d a(z) V |V|, \quad (2)$$

where most of the variables and coordinates follow standard meteorological conventions ( $x$  and  $U$  are streamwise and  $y$  and  $V$  spanwise components),  $\langle uu_j \rangle$  and  $\langle vu_j \rangle$  are Reynolds shear stresses,  $C_d$  is the drag coefficient, and  $a(z)$  is the building frontal area density. The Coriolis force is ignored in (1) and (2).

There have been many studies that use this drag-force approach to incorporate the aerodynamic effects of roughness elements on airflow over urban areas into mesoscale meteorological models (e.g., Masson 2006). Otte et al. (2004) compared mesoscale meteorological simulations of temperature, wind speed and direction, and the height of the planetary boundary layer with observations and concluded that the drag approach is better than the roughness-length approach. Recent studies have revised and extended the drag approach in urban meteorological modeling (Hamdi and Masson 2008; Masson and Seity 2009).

In spite of the successes of these drag approaches, a serious issue is encountered when determining the values of drag coefficients for urban areas with highly complex surface geometries. Santiago et al. (2008) performed Reynolds-averaged Navier–Stokes simulations to evaluate the values of drag coefficients for obstacle arrays with simple surface geometry that consists of cubic buildings with a uniform height over a wide range of roughness densities; they indicated that the drag coefficient ranges from 0.6 to 1.5. In contrast, Hagishima et al. (2009) examined the values of drag coefficients for building arrays with variable heights from wind-tunnel experiments and indicated that the values for variable-height buildings, particularly in cases with large roughness densities, are significantly larger than those for building arrays with uniform heights. In real cities,

TABLE 1. Calculated roughness parameters for London, Toulouse, Berlin, Salt Lake City, Los Angeles (Ratti et al. 2002), and central Tokyo.

	London	Toulouse	Berlin	Salt Lake City	Los Angeles	Central Tokyo
$h_{av}$ (m)	13.6	15.3	18.6	16.3	51.3	18.4
$V_h$ (-)	0.37	0.40	0.23	0.87	1.00	0.93
$\lambda_f$ (-)	0.32	0.32	0.23	0.11	0.45	0.39

building heights are highly variable and building densities large; standard deviations in building height are equal to the average building height for some urban areas (Ratti et al. 2002). Therefore, it is not easy to determine drag coefficients for roughness in actual urban areas. In other words, the drag-force approach may not be appropriate in incorporating the aerodynamic effects of roughness elements for cases of real urban areas, since this approach assumes that urban roughness is approximated as having simplified surface geometries.

In this way, important issues still remain in the representation of urban surface forms in numerical modeling using both the roughness-length and drag-force approaches. To deal with atmospheric flows over actual urban areas consisting of a complex of high-rise and low-rise buildings with variable packing densities, the roughness-length approach somehow needs to take into consideration the characteristics of urban surface geometry, while the drag-force approach requires variable drag coefficients evaluated by considering the complex geometry of urban surfaces.

The purpose of this study is to derive aerodynamic properties for airflows over complex roughness obstacles whose configuration is based on the features of realistic urban areas. We first examine the building morphological characteristics of building heights and roughness densities for actual cities. This analysis is used to set up obstacle arrays that represent realistic urban surface geometries for large-eddy simulations (LESs) of turbulent flows over various urban-type roughness surfaces. By performing a set of LESs, we investigate the relationship between the aerodynamic roughness parameters and building morphological characteristics. Possible applications of the roughness-length and drag-force approaches in mesoscale meteorological models are then discussed by investigating the spatial distributions of roughness parameters over central Tokyo.

## 2. Building morphological characteristics of actual urban areas

We investigate building morphological characteristics in a 36-km<sup>2</sup> (6 km × 6 km) area of central Tokyo, Japan, as a case study for an actual urban area, using data on building heights (above ground level) resolved at 2-m

intervals in a Geographic Information Systems (GIS) dataset (Kokusai Kogyo Co., Ltd.).

Table 1 shows and compares some of the roughness parameters, such as average building height  $h_{av}$ , building height variability  $V_h$ , and building frontal area index  $\lambda_f$ , for London, England; Toulouse, France; Berlin, Germany; Salt Lake City, Utah; Los Angeles, California (Ratti et al. 2002); and central Tokyo. The values of  $V_h$  and  $\lambda_f$  are defined, respectively, as the ratio of the standard deviation of building height to the average building height and the ratio of the total frontal area of roughness elements to the total surface area. The  $h_{av}$  values are similar in the European cities, Salt Lake City, and central Tokyo, while that for Los Angeles is the largest of all the cities. The  $V_h$  values of the European cities are relatively small, ranging from 0.2 to 0.4, while those of the North American cities and central Tokyo are significantly larger, showing nearly 1.0. The  $\lambda_f$  values of all the cities range from 0.11 to 0.45. This quantitative analysis listed in Table 1 reveals the following: the characteristics of surface geometries of European cities are densely built up, consisting of buildings with nearly uniform heights; those of Los Angeles and central Tokyo are densely built up, consisting of buildings with very variable heights; and those of Salt Lake City are sparsely built up, having buildings with very variable heights. These facts indicate that it is quite difficult to generalize and design realistic urban surface geometries as regularly distributed obstacles with uniform heights. Therefore, aerodynamic roughness parameters need to be evaluated for various kinds of real urban areas with various building morphological characteristics.

Figure 2 shows the spatial distribution of building heights in the study area of central Tokyo. Most of the ground surface is covered with buildings and structures of various heights, except for the wide-open area of the Imperial Palace located in the center of the study area. High-rise buildings are densely distributed to the east and south of this open area, while they are more sparsely distributed in the northeast and southwest parts.

Figure 3 demonstrates the frequency distributions of building heights  $h$ ,  $h_{av}$ ,  $V_h$ , and  $\lambda_f$  in central Tokyo. The original data were smoothed out by taking moving averages with a 20-m window, after which the  $h_{av}$ ,  $V_h$ , and

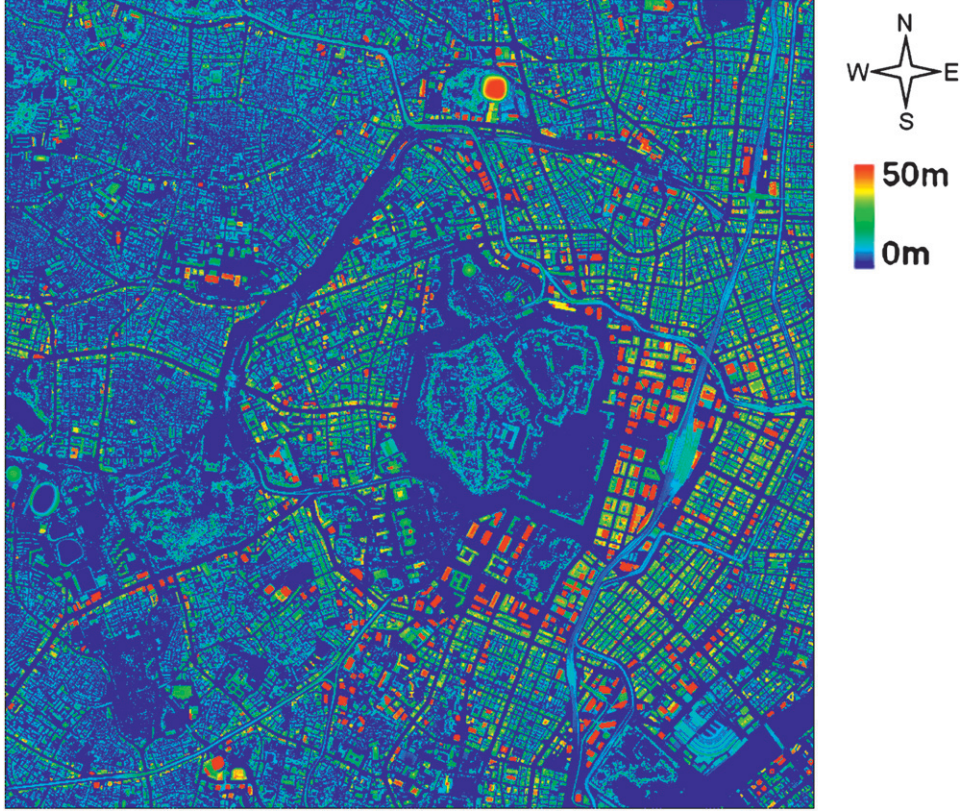


FIG. 2. Spatial distribution of building heights (color scale) in central Tokyo. The domain covers  $36 \text{ km}^2$ .

$\lambda_f$  values for 1-km $^2$  areas were evaluated by gradually moving the evaluation area in 20-m increments. Note that the average building heights here are defined as the values evaluated over each area of 1 km  $\times$  1 km. The  $h$  frequency is the largest in the range of 0.0–5.0 m and gradually decreases with the increase in building heights (Fig. 3a). It is also found that high-rise buildings with heights greater than 100 m do exist, albeit as only a small percentage. Corresponding to this height distribution, the frequency distribution of the area-mean height indicates a sharp peak in the range of 10–20 m and a rapid decrease with the  $h_{av}$  increase.

On the other hand, the variability of building height is quite large, as shown in Table 1. The frequency distribution of  $V_h$  is shown in Fig. 3c, indicating a peak in the range of 0.9–1.0 and an excess of 0.5 in almost all areas of central Tokyo. Furthermore, areas with  $V_h$  values greater than 1.0 amount to 13.4% of the total study area in central Tokyo. The frequency distribution of  $\lambda_f$  shows a peak in the range of 0.3–0.4; in particular,  $\lambda_f$  exceeds 0.4 over nearly half the area of central Tokyo. Therefore, the surface geometry of central Tokyo is found to be highly inhomogeneous and covered with low- and high-rise buildings with very variable heights. This type

of complex urban topology is modeled in the present LES as an obstacle array.

### 3. Computational method and settings

#### a. Numerical model

To perform an LES, a wind flow representing the characteristics of a turbulent boundary layer flow over rough surfaces needs to be generated in a computational domain. Figure 4 demonstrates a schematic diagram of the numerical model and the concept of generating turbulent flow. Two computational regions are set up. One is the driver region for generating a spatially developing turbulent boundary layer flow, and the other is the main computational region for examining turbulent flows over various types of building arrays. At the inlet boundary of the driver region, a uniform flow is imposed. To generate a thick turbulent boundary layer with sufficient turbulent fluctuation, roughness blocks are placed near the inlet of the driver region. A fully developed turbulent boundary layer flow at the exit boundary of the driver region is imposed at the inlet of the main computational domain at every time step. In this way, turbulent flow over building arrays is reproduced in the main region.

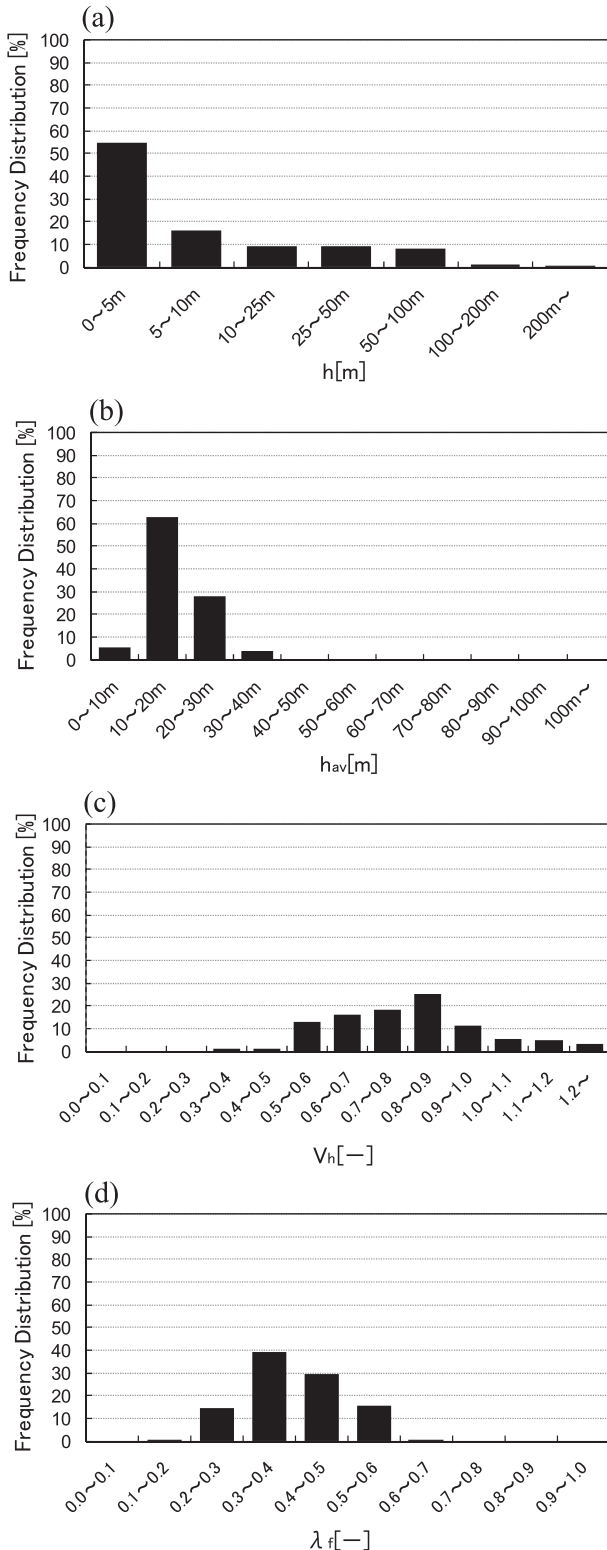


FIG. 3. Frequency distribution of roughness parameters for central Tokyo: (a) building height, (b) average building height, (c) building height variability, and (d) building frontal area index.

### b. Governing equations

The governing equations for the present LES are the filtered continuity equation and the filtered Navier–Stokes equation:

$$\frac{\partial \bar{u}_i}{\partial x_i} = 0, \quad (3)$$

$$\frac{\partial \bar{u}_i}{\partial t} + \bar{u}_j \frac{\partial \bar{u}_i}{\partial x_j} = -\frac{1}{\rho} \frac{\partial \bar{p}}{\partial x_i} + \frac{\partial}{\partial x_j} v \left( \frac{\partial \bar{u}_i}{\partial x_j} + \frac{\partial \bar{u}_j}{\partial x_i} \right) - \frac{\partial}{\partial x_j} \tau_{ij} + f_i, \quad (4)$$

$$\tau_{ij} = \bar{u}_i \bar{u}_j - \bar{u}_i \bar{u}_j, \quad (5)$$

$$\tau_{ij} - \frac{1}{3} \delta_{ij} \tau_{kk} = -\nu_{SGS} \bar{S}_{ij} \quad \text{and}$$

$$\nu_{SGS} = (C_s f_s \bar{\Delta})^2 (2 \bar{S}_{ij} \bar{S}_{ij})^{1/2}, \quad (6)$$

$$\bar{S}_{ij} = (\partial \bar{u}_i / \partial x_j + \partial \bar{u}_j / \partial x_i) / 2, \quad (7)$$

$$f_s = 1 - \exp \frac{-z^+}{25}, \quad \text{where } z^+ = \frac{zu^*}{\nu}, \quad (8)$$

and

$$\bar{\Delta} = (\bar{\Delta}_x \bar{\Delta}_y \bar{\Delta}_z)^{1/3}, \quad (9)$$

where  $u_i$ ,  $t$ ,  $p$ ,  $\rho$ ,  $\tau_{ij}$ ,  $\delta_{ij}$ ,  $\nu$ ,  $\nu_{SGS}$ , and  $u^*$  are wind velocity, time, pressure, density, subgrid-scale Reynolds stress, Kronecker delta, kinematic viscosity, eddy viscosity coefficient, and friction velocity, respectively. Subscripts  $i$  and  $j$  stand for coordinates (streamwise direction,  $x_1 = x$ ; spanwise,  $x_2 = y$ ; and vertical,  $x_3 = z$ ). Overbars indicate that the variable is spatially filtered. In this study, the standard Smagorinsky model (Smagorinsky 1963) is employed because of its simplicity and low computational cost. Here,  $C_s$  is set to 0.1. The Van Driest damping function (Van Driest 1956)  $f_s$  is used to reduce the subgrid-scale viscosity near the ground surface at which the no-slip condition is imposed. This damping function is commonly employed in an LES of flows over a flat lower boundary. The application of the damping function to highly rough surfaces, however, requires some caution, because it is difficult to appropriately estimate the friction velocity in separated flow regions around roughness obstacles. Although the present study follows the commonly used approach in dealing with the representation of the near-wall turbulence, further studies are necessary for modeling subgrid-scale effects in the near-wall region, which is outside the scope of the present paper. We use  $\bar{\Delta}$  to denote the grid-filter width. The body force  $f_i$  is included in the Navier–Stokes equations in order to incorporate

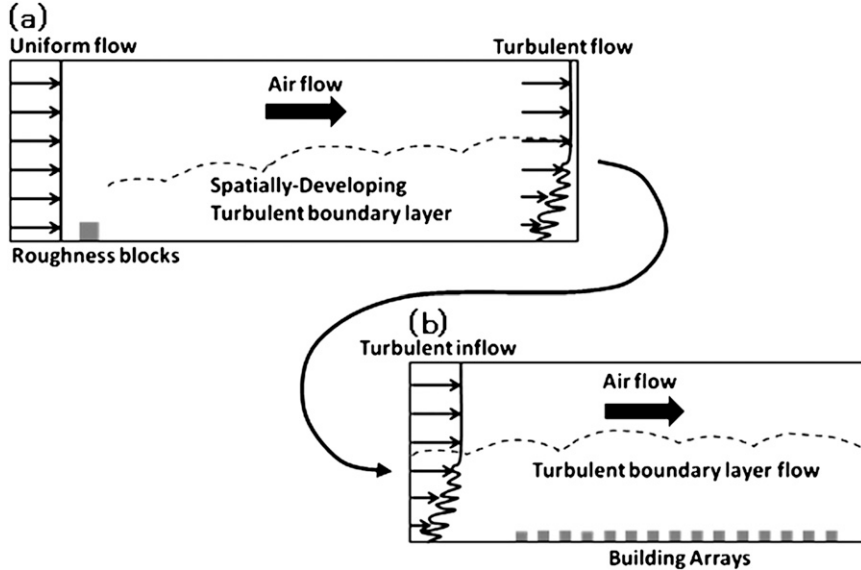


FIG. 4. Schematic diagram of the numerical model. (a) The driver region for generation of the spatially developing turbulent boundary layer flow. (b) The main region for turbulent flows over building arrays.

the effects of buildings on fluid flow. The feedback forcing formulation by Goldstein et al. (1993) is used to represent this body force:

$$f_i = \alpha \int_0^t u_i(t') dt' + \beta u_i(t), \quad \alpha < 0, \beta < 0, \quad (10)$$

where  $\alpha$  and  $\beta$  are negative constants. The stability limit is given by  $\Delta t < [-\beta - \sqrt{(\beta^2 - 2\alpha k)}]/\alpha$ , and  $k$  is a constant value of order 1.

### c. Computational method

The governing equations are discretized on a staggered grid system. The coupling algorithm of the velocity and pressure fields is based on the marker and cell (MAC) method (Chorin 1967) with the Adams-Bashforth scheme for time integration. The Poisson equation is solved by the successive overrelaxation (SOR) method. The spatial derivatives in the governing equation are discretized with a second-order-accurate central difference on the staggered mesh.

At the inlet boundary in the streamwise direction a uniform-flow condition is imposed, while at the exit boundary the Sommerfeld radiation condition is applied. At the top boundary, free-slip conditions for the streamwise and spanwise components are imposed and the vertical velocity component is zero. At the spanwise lateral boundaries, a periodic condition is imposed. At the ground surface, a nonslip condition is imposed for each velocity component. At the surfaces of the building bodies, the feedback forcing formulated by Goldstein

et al. (1993) is applied for its computational stability for turbulent flow around bluff bodies.

### d. Setting of urban-type building arrays

Many researchers have dealt with regular arrays of rectangular obstacles when investigating turbulence structures above a rough ground surface. For example, Cheng et al. (2007) conducted wind tunnel experiments on turbulent flows over staggered and aligned arrays of cubic buildings with  $\lambda_f = 0.0625$  and 0.25 and investigated the influence of the configuration and roughness density on turbulence characteristics and aerodynamic roughness parameters. Santiago et al. (2008) performed numerical simulations of turbulent flows over staggered arrays of cubic buildings with  $\lambda_f = 0.0625$ –0.44 and examined the variation in drag coefficient with  $\lambda_f$ . A common point in their studies is that the obstacles had uniform heights. However, from the building morphological analysis presented in section 2, it was demonstrated that the surface geometries of actual urban areas indicate a large variation not only in  $\lambda_f$  but also in  $V_h$  values. Therefore, in order to systematically investigate aerodynamic roughness parameters over various actual urban areas, urban-type surface geometries with a wide range of both  $\lambda_f$  and  $V_h$  values need to be examined.

In this study, we deal with a wide variety of square arrays of buildings as simplified surface geometry for an actual urban area by systematically changing the values of  $\lambda_f$  and  $V_h$ . Table 2 lists cases for the LESs of turbulent flows over various building arrays. Buildings are set

TABLE 2. Cases of urban-type building arrays used in LESs.

Case	$\lambda_f$	$h_{\max}$	$h_{\min}$	$V_h$	Geometry of a repeating unit
1	0.0625	$1.0 h_{\text{av}}$	$1.0 h_{\text{av}}$	0.0	Square array consisting of four cubic buildings
2	0.0625	$1.43 h_{\text{av}}$	$0.86 h_{\text{av}}$	0.25	Square array consisting of three lower buildings and one higher building
3	0.0625	$1.88 h_{\text{av}}$	$0.71 h_{\text{av}}$	0.50	
4	0.0625	$2.29 h_{\text{av}}$	$0.57 h_{\text{av}}$	0.75	
5	0.0625	$2.75 h_{\text{av}}$	$0.43 h_{\text{av}}$	1.0	
6	0.11	$1.0 h_{\text{av}}$	$1.0 h_{\text{av}}$	0.0	Square array consisting of four cubic buildings
7	0.11	$1.43 h_{\text{av}}$	$0.86 h_{\text{av}}$	0.25	Square array consisting of three lower buildings and one higher building
8	0.11	$1.88 h_{\text{av}}$	$0.71 h_{\text{av}}$	0.50	
9	0.11	$2.29 h_{\text{av}}$	$0.57 h_{\text{av}}$	0.75	
10	0.11	$2.75 h_{\text{av}}$	$0.43 h_{\text{av}}$	1.0	
11	0.16	$1.0 h_{\text{av}}$	$1.0 h_{\text{av}}$	0.0	Square array consisting of four cubic buildings
12	0.16	$1.43 h_{\text{av}}$	$0.86 h_{\text{av}}$	0.25	Square array consisting of three lower buildings and one higher building
13	0.16	$1.88 h_{\text{av}}$	$0.71 h_{\text{av}}$	0.50	
14	0.16	$2.29 h_{\text{av}}$	$0.57 h_{\text{av}}$	0.75	
15	0.16	$2.75 h_{\text{av}}$	$0.43 h_{\text{av}}$	1.0	
16	0.25	$1.0 h_{\text{av}}$	$1.0 h_{\text{av}}$	0.0	Square array consisting of four cubic buildings
17	0.25	$1.43 h_{\text{av}}$	$0.86 h_{\text{av}}$	0.25	Square array consisting of three lower buildings and one higher building
18	0.25	$1.88 h_{\text{av}}$	$0.71 h_{\text{av}}$	0.50	
19	0.25	$2.29 h_{\text{av}}$	$0.57 h_{\text{av}}$	0.75	
20	0.25	$2.75 h_{\text{av}}$	$0.43 h_{\text{av}}$	1.0	
21	0.33	$1.0 h_{\text{av}}$	$1.0 h_{\text{av}}$	0.0	Square array consisting of four cubic buildings
22	0.33	$1.43 h_{\text{av}}$	$0.86 h_{\text{av}}$	0.25	Square array consisting of three lower buildings and one higher building
23	0.33	$1.88 h_{\text{av}}$	$0.71 h_{\text{av}}$	0.50	
24	0.33	$2.29 h_{\text{av}}$	$0.57 h_{\text{av}}$	0.75	
25	0.33	$2.75 h_{\text{av}}$	$0.43 h_{\text{av}}$	1.0	
26	0.44	$1.0 h_{\text{av}}$	$1.0 h_{\text{av}}$	0.0	Square array consisting of four cubic buildings
27	0.44	$1.43 h_{\text{av}}$	$0.86 h_{\text{av}}$	0.25	Square array consisting of three lower buildings and one higher building
28	0.44	$1.88 h_{\text{av}}$	$0.71 h_{\text{av}}$	0.50	
29	0.44	$2.29 h_{\text{av}}$	$0.57 h_{\text{av}}$	0.75	
30	0.44	$2.75 h_{\text{av}}$	$0.43 h_{\text{av}}$	1.0	

squarely arrayed with various combinations of  $\lambda_f$  and  $V_h$  by changing the  $\lambda_f$  value between 0.0625 and 0.44 and the  $V_h$  value between 0.0 and 1.0. The values of  $h_{\max}$  and  $h_{\min}$  shown in Table 2 represent higher- and lower-building heights, namely  $(1.0\text{--}2.75) \times h_{\text{av}}$  and  $(0.43\text{--}1.0) \times h_{\text{av}}$ , respectively. In total, the study examines 30 cases of urban-type building arrays with  $\lambda_f = 0.0625\text{--}0.44$  and  $V_h = 0.0\text{--}1.0$ .

Figure 5 shows the configuration of the square array of buildings in the case of  $\lambda_f = 0.0625$ . A unit of the building array shown in Fig. 5 consists of one higher and three lower buildings over an area of  $8.0 h_{\text{av}} \times 8.0 h_{\text{av}}$ . Each unit of other building arrays not shown here consists of one higher and three lower buildings over areas of  $6.0 h_{\text{av}} \times 6.0 h_{\text{av}}$ ,  $5.0 h_{\text{av}} \times 5.0 h_{\text{av}}$ ,  $4.0 h_{\text{av}} \times 4.0 h_{\text{av}}$ ,  $3.5 h_{\text{av}} \times 3.5 h_{\text{av}}$ , and  $3.0 h_{\text{av}} \times 3.0 h_{\text{av}}$ , with  $\lambda_f$  values of 0.11, 0.16, 0.25, 0.33, and 0.44, respectively. The average building height is set to be constant under the same  $\lambda_f$  values. The details for these settings are given in the computational domain (see section 3e).

In addition to the square arrays of buildings, a staggered array of buildings is also set in order to validate the present LES model against previous experimental

and numerical studies (Cheng et al. 2007; Santiago et al. 2008). For the staggered array cases, the building height is uniform (i.e.,  $V_h = 0$ ) and  $\lambda_f$  is changed from 0.0625 to 0.44 (as in the square array cases).

#### e. Computational domain

It is important to design the computational domain size and grid resolution when performing LESs of turbulent flow over building arrays, by trading off computational cost, efficiency, and accuracy. Santiago et al. (2008) set up a computational domain with a length of  $(3.0\text{--}8.0) h$ , a width of  $(1.5\text{--}4.0) h$ , and a height of  $4.0h$ , where  $h$  was the size of the cubic obstacle in the range of  $0.0625 < \lambda_f < 0.44$ , in order to systematically estimate the drag around individual buildings. In their simulations, each building was resolved by 16 grid points in each direction. Kanda (2006) used a larger computational domain (a length of  $(7.0\text{--}18.2) h$ , a width of  $(6.0\text{--}7.8) h$ , and a height of  $6.0 h$ ) in the range of  $0.03 < \lambda_f < 0.44$  in order to capture turbulent organized structures above the canopy, while their resolution for each building was less than 10 grid points in each dimension.

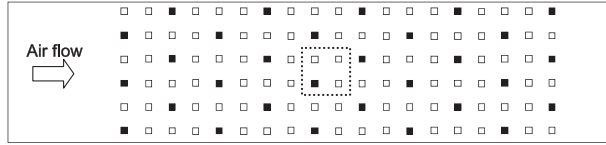


FIG. 5. Plan view of the building array in the main computational domain. The dotted line indicates the area of repeating units comprising one higher and three lower buildings. The black and white squares represent higher and lower buildings, respectively.

In contrast, to evaluate both roughness length and drag coefficient by representing the overall structure of the turbulent boundary layer, the computational domain size needs to be made much larger than the building scale, by maintaining an appropriate number of grid points within each building. For example, the lateral scale of the computational domain should be larger than twice the scale of the turbulent boundary layer (Jimenez 2004), while each building should be resolved by at least 15–20 grid points in each dimension in order to accurately evaluate the drag around a building (Xie and Castro 2006; Santiago et al. 2008). Both requirements, however, need an extensive computational resource. On the other hand, Bou-Zeid et al. (2009) indicated that sensitive analysis for turbulent flows over complex surface geometries is expected to be reliable even with a lower resolution of four grids across obstacles. In addition, Tseng et al. (2006) mentioned that the basic turbulent flow patterns around a bluff body can be simulated even with four grid points across a building, although this grid size seems to be marginal. Thus, their resolution of four grids across obstacles is still considered to be sufficient for examining the sensitivities of flows over various distributions of buildings.

Based on these previous studies, we set the main computational domain with a length ( $x_1$ ) of  $8.0 \delta$  ( $\delta$ , turbulent boundary layer thickness), a width ( $x_2$ ) of  $2.0 \delta$ , and a height ( $x_3$ ) of  $4.0 \delta$ . Each building is resolved by  $4 \times 4 \times 11$  grid points in the streamwise, spanwise, and vertical directions, due to limitations of computational resources. Building arrays with  $\lambda_f = 0.0625, 0.11, 0.16, 0.25, 0.33$ , and  $0.44$  consisted of  $19 \times 6, 26 \times 8, 31 \times 8, 38 \times 12, 44 \times 12$ , and  $51 \times 16$  arrays in the streamwise and spanwise directions, respectively. The first row of building array in each case is placed at a  $20 h_{av}$  distance downstream of the inlet of the main computational domain. The number of grid points in the main computational region is  $400 \times 96 \times 90$ . In addition, the size of the driver region is  $20.0 \delta \times 2.0 \delta \times 4.0 \delta$  in  $x_1, x_2$ , and  $x_3$ , respectively.

#### 4. Validation of the LES model

In this section, the LES results for the characteristics of turbulent flows and aerodynamic roughness parameters over regular arrays of cubic buildings are compared with the experimental study by Cheng et al. (2007) and the numerical study by Santiago et al. (2008), in order to examine and confirm the validity of this LES model. In their experiments, Cheng et al. examined flows over an aligned array for which the blocks were aligned in the streamwise direction but staggered in the spanwise direction (see Fig. 6b). On the other hand, the present study examines a square array (see Fig. 6c). Although an aligned array is not exactly the same as a square array, Coceal et al. (2006) showed from a direct numerical simulation (DNS) that there are few differences in the vertical profiles of mean wind velocity and Reynolds

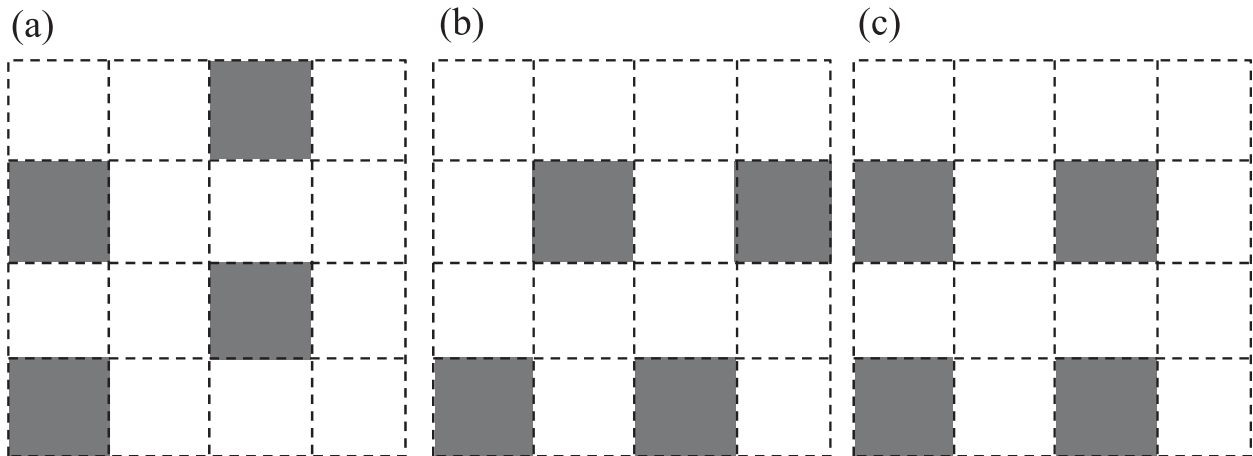


FIG. 6. Plan view of the surface geometries of various building arrays: (a) staggered, (b) aligned, and (c) square arrays. The streamwise direction in all cases is left to right. [Adapted from Coceal et al. (2006).]

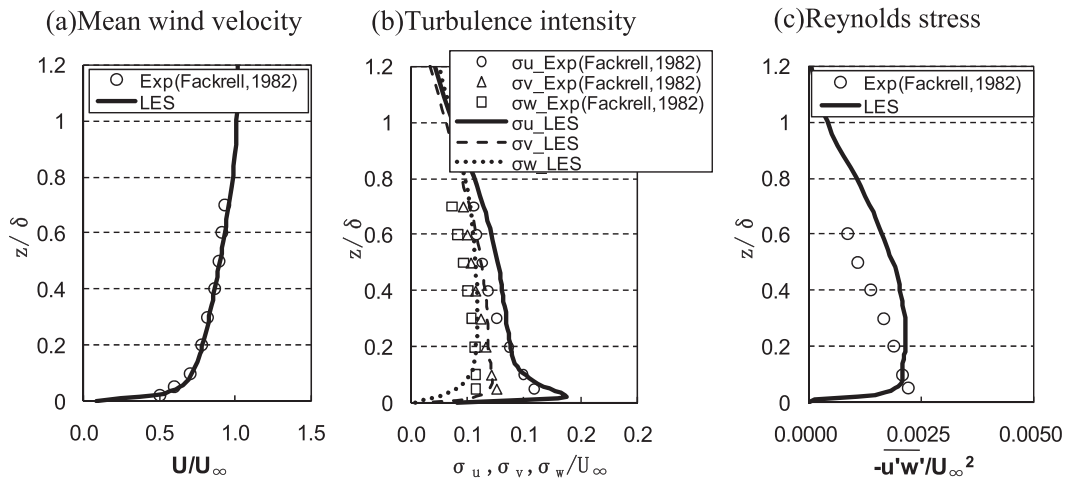


FIG. 7. Turbulence characteristics of the approaching flow: (a) vertical profiles of mean wind velocity, (b) vertical profiles of turbulence intensity, and (c) vertical profiles of Reynolds stress.

stress between square and aligned arrays of buildings. Thus, the results produced by Cheng et al. are used here.

First, the inflow turbulence characteristics obtained near the exit of the driver region are validated. The wind tunnel flow of Fackrell and Robins (1982) is used here for comparison. Figure 7 compares the LES results with their experimental results. The profile of the mean wind velocity is found to fit the experimental profile of a 0.14 power law, which indicates that sufficient turbulence intensities comparable to the experiments are obtained. The Reynolds stress profile exhibits a constant in the range of  $z/\delta = 0.1\text{--}0.5$ , while that of Fackrell and Robins (1982) decreases with height. In the present LES model, turbulent boundary layer flow was generated by roughness blocks placed on the ground surface with a long fetch (20.0  $\delta$ ), while in the wind tunnel experiment by Fackrell and Robins (1982) the turbulent flow was generated by vortex generators with a short fetch (6.7  $\delta$ ). By setting a longer fetch than that of the wind tunnel experiment, fully developed turbulent boundary layer flow with a constant profile of Reynolds stress was obtained.

This unsteady wind flow is imposed at the inlet of the main region at each time step. In the following sections, turbulence characteristics and aerodynamic roughness parameters over building arrays in the area of an equilibrium state are investigated in comparison with those of Cheng et al. (2007) and Santiago et al. (2008).

#### a. Vertical profiles of mean wind velocity and Reynolds stress

In the LESs, sampling for statistical averaging started at a dimensionless time  $3.75 \delta/U_\infty$  ( $U_\infty$ , a free-stream

velocity) after achieving equilibrium states. The averaging time was set at  $6.25 \delta/U_\infty$  to obtain turbulence statistics data.

Figure 8 compares the results of vertical profiles of a spatially averaged mean wind velocity in the area of an equilibrium state over the staggered arrays of buildings with  $\lambda_f = 0.0625$  and 0.25 with the wind-tunnel experimental data of Cheng et al. (2007). Mean wind velocity is normalized by  $U_\infty$ . In the case of  $\lambda_f = 0.0625$ , the mean wind velocity profile of LES is similar to that obtained by the previous experiment in the range of  $z/h_{av} = 1.0$  to 2.5. At heights greater than  $z/h_{av} = 2.5$ , the difference in mean wind velocity between LES and the experiment becomes larger with height. In the case of  $\lambda_f = 0.25$ , the mean wind velocity profile is also similar in magnitude to that obtained by the experiment in the range of  $z/h_{av} = 1.0\text{--}2.5$ . However, at heights greater than  $z/h_{av} = 2.5$ , the difference in mean wind velocity between the LES and the experiment becomes larger with height. It should be noted that the ratios of the boundary layer thickness to the building height in the experiments by Cheng et al. and the present LES model were 6.0–7.0 and 13.0, respectively. Therefore, the difference in mean wind velocities at heights greater than  $z/h_{av} = 2.5$  is considered to be due to the difference in the ratio of the boundary layer thickness to building height.

Figure 9 compares the results of the vertical profile of the Reynolds stress in the area over the staggered arrays of buildings with  $\lambda_f = 0.0625$  and 0.25 with the experimental data of Cheng et al. (2007). The decrease in Reynolds stress with height in the wind-tunnel experiments is well represented in the present LES, in the range of  $z/h_{av} = 1.0\text{--}5.0$ .

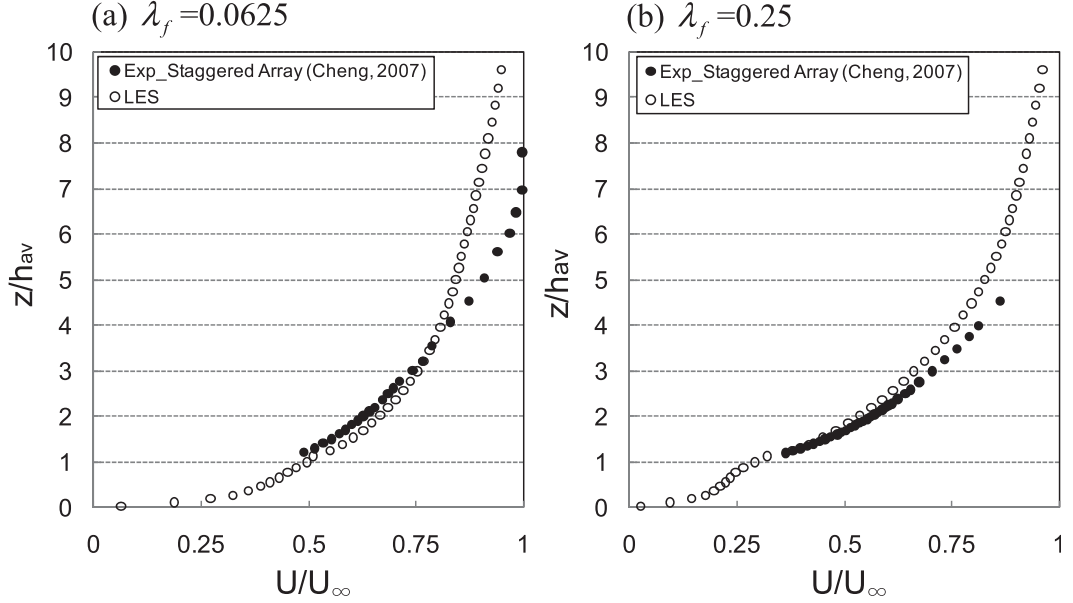


FIG. 8. Vertical profiles of mean wind velocity obtained by the present LES and the experiments of Cheng et al. (2007) for cases of  $\lambda_f$  = (a) 0.0625 and (b) 0.25.

### b. Variation in $z_0$ with $\lambda_f$

The relationship between roughness length and frontal area index is examined here. We evaluated  $z_0$  by fitting the computed mean wind velocity profiles to log law using the following expression:

$$u = \frac{u^*}{\kappa} \ln\left(\frac{z - d}{z_0}\right), \quad (11)$$

where the von Karman constant  $\kappa$  is 0.41 and  $u^*$  is determined from the surface shear stress  $\tau$  via

$$u^* = \sqrt{\tau/\rho}. \quad (12)$$

Here,  $\tau$  is obtained from the drag force evaluated for each unit area of a building array, using the procedure

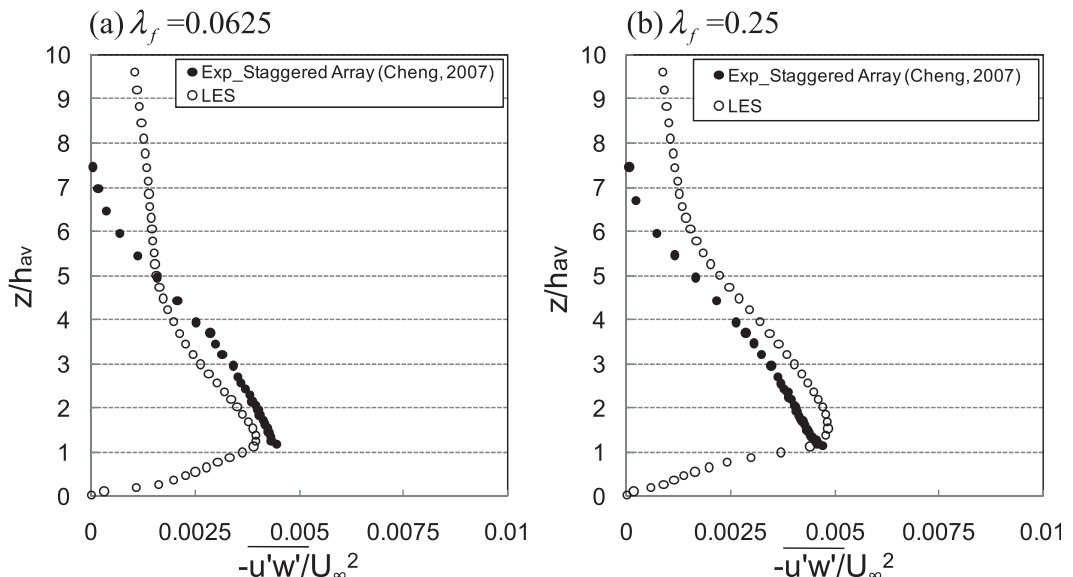


FIG. 9. As in Fig. 8, but for Reynolds stress.

shown by Martilli and Santiago (2007), and is expressed as follows:

$$\tau = \rho \frac{h_{\max}}{N_z} \sum_{k=1,N_z} D_k, \quad (13)$$

where  $N_z$  is the number of grid points in the vertical direction below the maximum building height. In this equation,  $D_k$  stands for the drag force at level  $k$  and is computed as

$$D_k = \frac{1}{(L_x L_y \Delta z_k - h_x h_y \Delta z_k)} \sum_{j=\text{js,je}} \Delta \bar{P}_{j,k} \frac{h_{\max}}{N_y} \Delta z_k, \quad (14)$$

where  $h_x$ ,  $h_y$ ,  $L_x$ ,  $L_y$ ,  $N_y$ ,  $\Delta \bar{P}_{j,k}$ , and  $\Delta z_k$  are the building length, the building width, the length of the repeating unit area, the width of the unit area, the number of grid points in the spanwise direction, the averaged pressure difference between the front and back of a building, and the grid size at level  $k$ , respectively.

The value of  $d$  is determined from the centroid of the drag force via (Jackson 1981)

$$d = \frac{\sum_{k=1,N_z} z_k D_k}{\sum_{k=1,N_z} D_k}. \quad (15)$$

Figure 10 shows variation in the normalized roughness length ( $z_0/h_{\text{av}}$ ) over the staggered arrays of buildings with  $\lambda_f$ . In Fig. 10, the estimates of the roughness length from the present LESs are also compared with the wind-tunnel experiments of Cheng et al. (2007) and the theoretical values based on the analytical model of Macdonald et al. (1998). It is indicated that the  $z_0/h_{\text{av}}$  values from LES agree well with the experimental results of Cheng et al. On the other hand, the present results generally underestimate the theoretical values from Macdonald's model. However, the overall tendency in the  $z_0/h_{\text{av}}$  change from Macdonald et al.'s (1998) theoretical model in which the value has a peak at around 0.2 seems to be reproduced in the present LES.

Cheng et al. (2007) considered that there were two possible reasons why the roughness lengths reproduced by the wind-tunnel experiments were smaller than those from the theoretical model of Macdonald et al. One was the difference in the fetch, and the other was the difference in the method of averaging wind velocity profiles when estimating roughness lengths. The length of fetch in the experiments by Cheng et al. was 150  $h$ , while the theoretical estimates in Macdonald et al. were validated against the wind-tunnel experiments with a shorter fetch (22  $h$ ): the fetch in Cheng et al. was much larger than

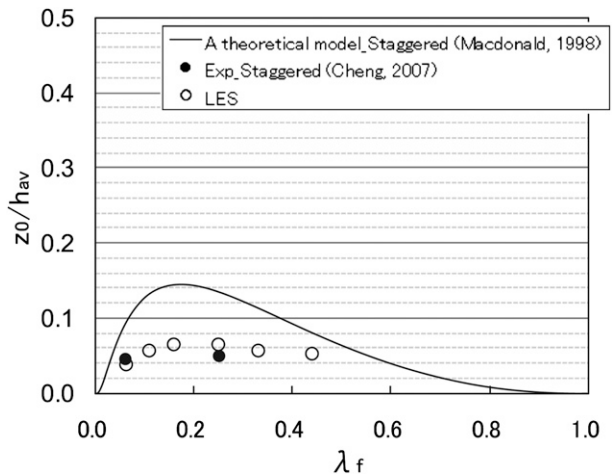


FIG. 10. Variations of  $z_0/h_{\text{av}}$  with  $\lambda_f$  for the staggered array of cubic buildings. The solid line indicates the relationship obtained from a theoretical model for a staggered array of cubic obstacles (Macdonald et al. 1998). The black circle indicates the experimental data of Cheng et al. (2007) in cases of  $\lambda_f = 0.0625$  and 0.25.

that in Macdonald et al. In addition, Cheng et al. evaluated roughness lengths by spatially averaging the velocity profiles over the area of a repeating unit of the building arrays, while Macdonald et al. used the experimental data for five different lateral locations in building arrays. Thus, the estimates by Cheng et al. were more representative of the aerodynamic surface roughness feature. Our roughness-length estimates were obtained from spatially representative data over the computational domain with a long fetch comparable to the length in Cheng et al. Therefore, the present results are more consistent with the experimental data of Cheng et al.

### c. Variation in drag coefficient with $\lambda_f$

The variation in drag coefficients against the difference in  $\lambda_f$  is evaluated here. Total drag formally consists of the pressure difference between the frontal and back faces of each individual building and the surface drag. In this study, the frictional component of the surface drag is neglected in estimating the total drag force. This assumption is considered to be reasonable for densely distributed arrays but may be less true for sparsely distributed arrays, because of the relatively coarse resolution used in the present simulations. To validate the drag coefficient values of the present LESs, we follow the analysis procedures of Santiago et al. (2008), who estimated the drag coefficient determined by spatially averaging the sectional drag coefficient ( $\overline{Cd}$ ) via

$$\overline{Cd} = \frac{1}{h_{\max}} \int_0^{h_{\max}} Cd(z) dz. \quad (16)$$

Santiago et al. (2008) evaluated the sectional drag coefficient using total kinetic energy ( $q_{\text{tot}}$ ), based on the method of Martilli and Santiago (2007). Therefore, we also use the same method as used by Santiago et al. (2008). The formulation by Martilli and Santiago (2007) is

$$Cd(z) = -\frac{2\Delta \langle \bar{p}(z) \rangle}{\rho q_{\text{tot}}(z)} \frac{|U(z)|}{U(z)}. \quad (17)$$

Total velocity is decomposed as follows (Coceal et al. 2006):

$$u = U + \tilde{u} + u', \quad (18)$$

where  $U$  is the temporally and spatially averaged velocity,  $\tilde{u} = \bar{u} - U$  is the spatial variation in the temporal averaged velocity  $\bar{u}$ , and  $u' = u - U - \tilde{u}$  represents the turbulent fluctuation. Using these three velocity scales,  $q_{\text{tot}}(z)$  is defined as

$$q_{\text{tot}}(z) = U(z)^2 + \nu_{\text{TKE}}^2(z) + \nu_{\text{DKE}}^2(z), \quad (19)$$

where  $\nu_{\text{TKE}}(z)$  and  $\nu_{\text{DKE}}(z)$  indicate the spatially averaged turbulence kinetic energy and dispersive kinetic energy, respectively:

$$\nu_{\text{TKE}}^2(z) = 2\langle k \rangle, \quad \langle k \rangle = \frac{1}{2}(\langle u'(z)^2 \rangle + \langle v'(z)^2 \rangle + \langle w'(z)^2 \rangle), \quad (20)$$

and

$$\nu_{\text{DKE}}^2(z) = 2\langle e \rangle, \quad \langle e \rangle = \frac{1}{2}(\langle \tilde{u}(z)^2 \rangle + \langle \tilde{v}(z)^2 \rangle + \langle \tilde{w}(z)^2 \rangle). \quad (21)$$

Figure 11 compares the variations in  $\overline{Cd}$  with  $\lambda_f$  in the present LES with the results produced by Santiago et al. (2008) and Maruyama (1993). In the study by Maruyama (1993), numerical simulations of turbulent flows were performed over an urban canopy where buildings were not explicitly resolved but treated as a porous medium using a refined  $k-\epsilon$  turbulence model formulated by Hiraoka (1993); the drag coefficient values were estimated by fitting the computational results with the wind-tunnel experimental results of turbulent flows over the staggered arrays of cubic buildings for various  $\lambda_f$ . In Fig. 11, the  $\overline{Cd}$  value of LES increases with  $\lambda_f$  until about  $\lambda_f = 0.16$  and then decreases with  $\lambda_f$ . The LES results fall in the range between the two other studies and generally agreed well with their results. Specifically, the variation in  $\overline{Cd}$  with  $\lambda_f$  obtained from the present LES is similar to those of the previous studies.

Although four grid points across a building in the present LES model may be a little too coarse for an accurate simulation of pressure forces, it is considered

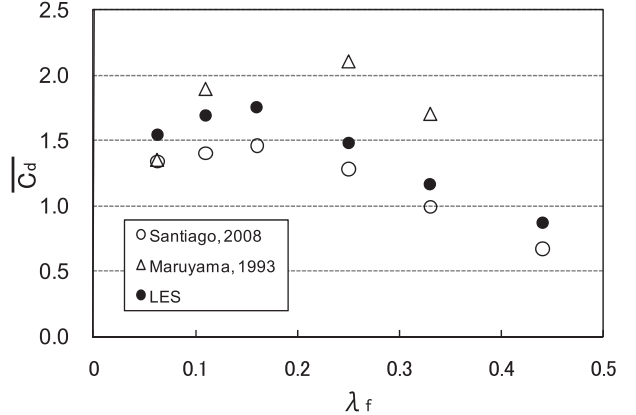


FIG. 11. Variations of  $\overline{Cd}$  with  $\lambda_f$  for the staggered array of cubic buildings. The results of the present LES (black circles), Santiago et al. (2008) (white circles), and Maruyama (1993) (triangles) are indicated.

that the basic characteristics of turbulent flows over various types of building arrays in this LES model were successfully simulated from a comparison of the present LES with previous numerical and wind-tunnel data.

## 5. LES results

### a. Turbulence characteristics over building arrays with various $\lambda_f$ and $V_h$

Figure 12 shows the vertical profiles of the mean wind velocity obtained from the present LESs. For reference, Fig. 12 also indicates the wind-tunnel experiments of Cheng et al. (2007) for flows over an aligned array of cubic blocks (i.e., uniform height) with  $\lambda_f = 0.0625$  and 0.25. As has already been indicated in Fig. 8 for the staggered array cases, the LES results in the case of  $\lambda_f = 0.0625$  and 0.25 at  $V_h = 0.0$  for the square arrays seem to be consistent with the experimental results. In cases with building height variability (i.e.,  $V_h \neq 0$ ) for various  $\lambda_f$ , mean wind velocities gradually decrease with the increase in  $V_h$  at levels of  $z/h_{\text{av}} > 1.0$ , owing to the existence of higher buildings, while there are few differences in velocity among the various  $V_h$  cases at levels of  $z/h_{\text{av}} < 1.0$ . Furthermore, with the increase in both  $\lambda_f$  and  $V_h$ , mean wind velocities are seen to gradually decrease and show nearly constant values at levels up to the top of the highest building (i.e.,  $1.0 < z/h_{\text{av}} < 2.0$ ).

Figure 13 shows the vertical profiles of Reynolds stress in the LESs as well as those obtained from the wind-tunnel experiments by Cheng et al. (2007). The results with uniform-height buildings at  $\lambda_f = 0.0625$  and 0.25 agree well with the experiments of Cheng et al. in the lower part of the boundary layer. Note that the values of Reynolds stress for these  $V_h = 0$  cases are a little

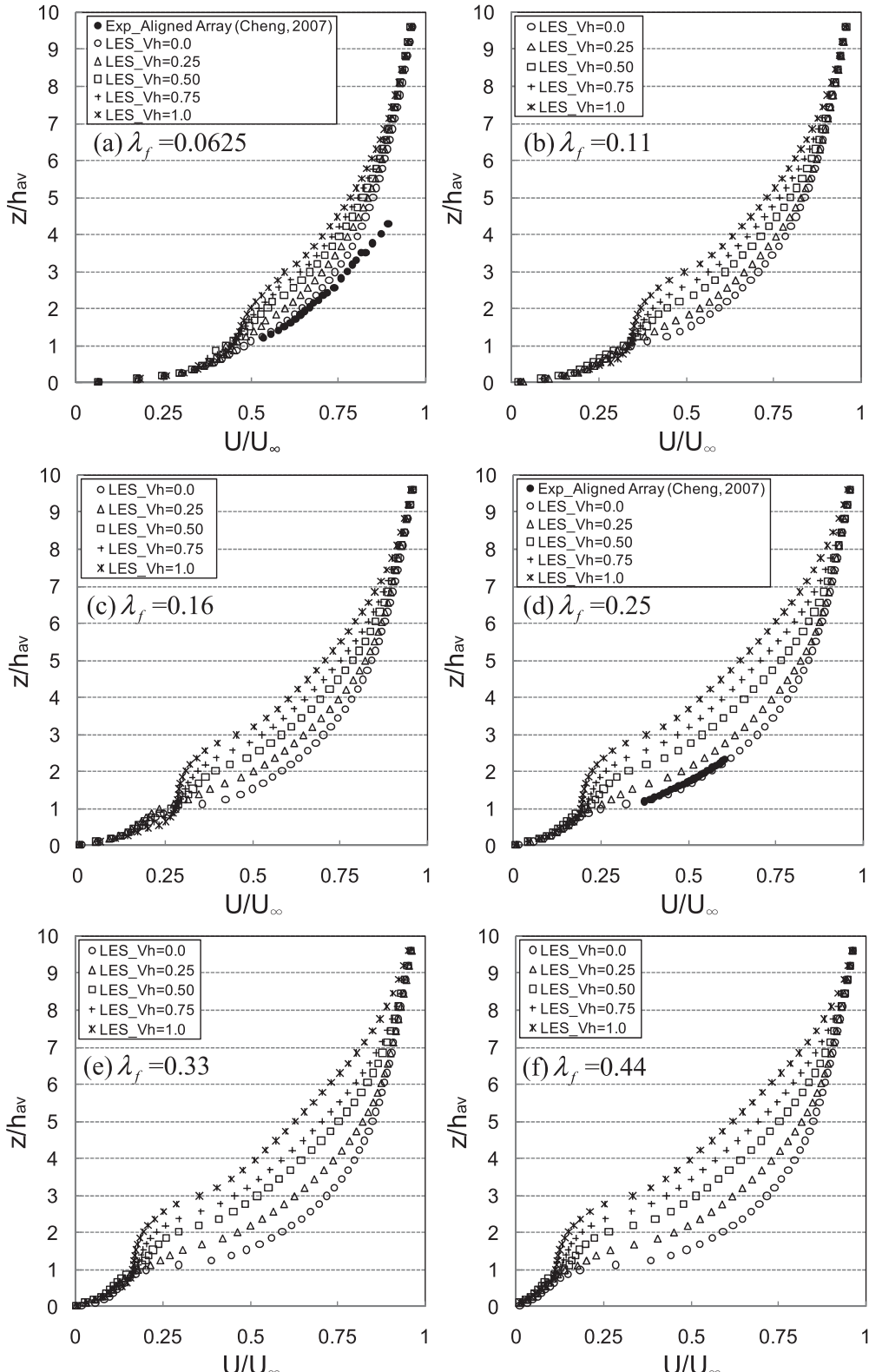


FIG. 12. Vertical profiles of mean wind velocity for  $\lambda_f$  values at (a) 0.0625, (b) 0.11, (c) 0.16, (d) 0.25, (e) 0.33, and (f) 0.44 with various  $V_h$  values. The results of the wind-tunnel experiment by Cheng et al. (2007) are also plotted in (a) and (d).

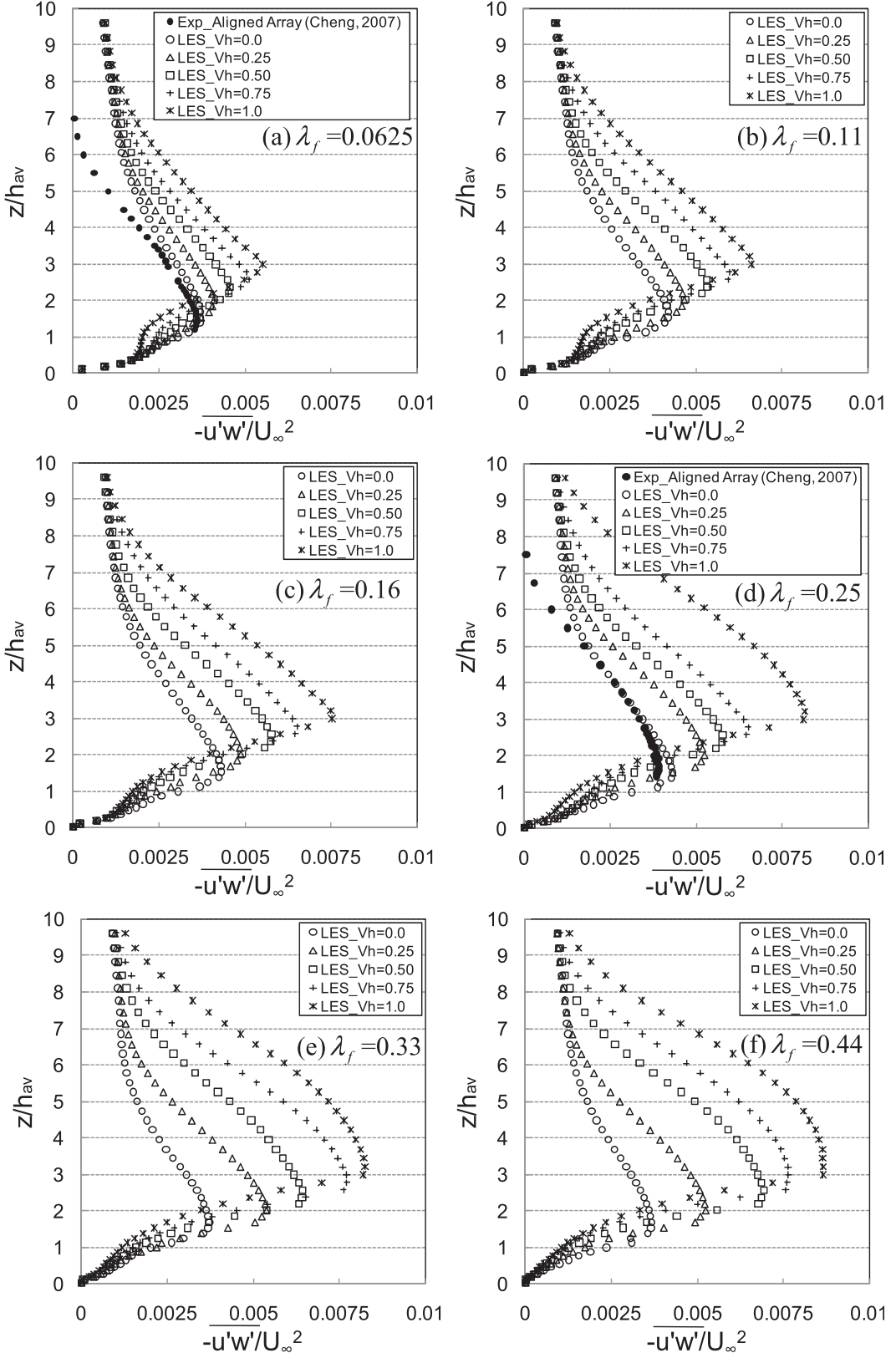


FIG. 13. As in Fig. 12, but for Reynolds stress.

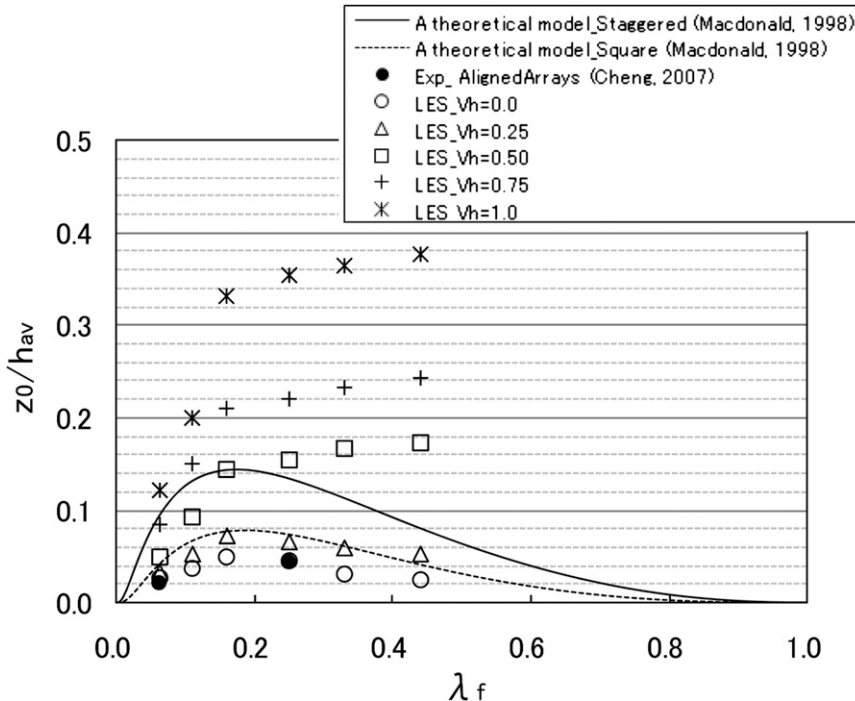


FIG. 14. Variations of  $z_0/h_{av}$  with  $\lambda_f$  and  $V_h$  obtained from the present LESs for  $V_h = 0.0, 0.25, 0.50, 0.75$ , and  $1.0$ ; the experiment of Cheng et al. (2007); and the theoretical model of Macdonald et al. (1998).

different from the results shown in Fig. 9, owing to the difference in the configuration of the building arrays (i.e., square versus staggered).

The results shown in Fig. 13 further indicate that, with the increase in  $V_h$ , the peak value of Reynolds stress becomes larger and exists at a higher level, which corresponds to the level of the higher building top; these features are found for every  $\lambda_f$  case. At the same time, with the increase in  $\lambda_f$  while the  $V_h$  value remained the same, the peak of the Reynolds stress becomes larger. Furthermore, the Reynolds stress is found to be consistently larger in the upper domain (approximately divided at  $2.5z/h_{av}$ ) with increasing  $V_h$ . These characteristics of the Reynolds stress variation indicate that the influence of higher buildings on the upper portion of the turbulent boundary layer is more pronounced in a higher  $V_h$  case. In this way, the highest building significantly affects and controls the turbulence characteristics.

#### b. Variation in roughness length and drag coefficient with $\lambda_f$ and $V_h$

Roughness length is an important parameter and is hence commonly used to describe surface aerodynamic characteristics, while drag coefficient is particularly useful for rough surfaces with urbanlike obstacles. In

this section, therefore, we examine the variations in roughness length  $z_0/h_{av}$  and drag coefficient  $\overline{Cd}$  in response to the changes in  $\lambda_f$  and  $V_h$ .

Figure 14 compares the variations in  $z_0/h_{av}$  against the values of  $\lambda_f$  and  $V_h$  obtained from the present LESs, the experiment of Cheng et al. (2007), and the theoretical model of Macdonald et al. (1998). The LES results with  $V_h = 0$  are seen to agree well with the experiment of Cheng et al. and to be comparable to the theoretical values for square arrays found by Macdonald et al.

For cases with building height variability,  $z_0/h_{av}$  values in the case of  $\lambda_f \leq 0.16$  and  $V_h \leq 0.5$  appear to be distributed in accordance with the theoretical curves proposed by Macdonald et al. within the difference in the building configuration. In the case of  $\lambda_f > 0.16$  and/or  $V_h > 0.5$ , on the other hand, the discrepancy in the  $z_0/h_{av}$  values between the LESs and the theory becomes more significant. The  $z_0/h_{av}$  value increased uniformly with the increase in  $\lambda_f$  for each  $V_h$  case; in particular, the results with  $V_h = 1.0$  indicate that the  $z_0/h_{av}$  values are about 3 times as large as the theoretical values. These characteristics of the  $z_0/h_{av}$  variation seen in Fig. 14 were also consistent with the results of wind-tunnel experiments in the study by Hagishima et al. (2009), who examined flows over staggered building arrays with uniform ( $V_h = 0.0$ ) and nonuniform ( $V_h = 0.58$ ) heights.

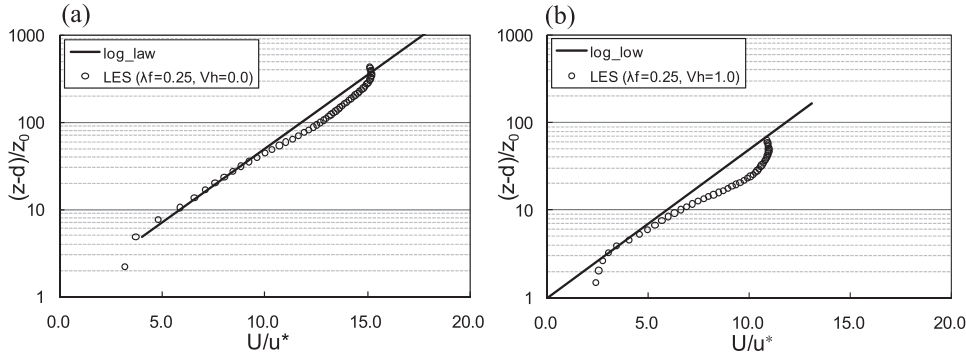


FIG. 15. Fitted log-law profiles for cases of (a)  $\lambda_f = 0.25$  and  $V_h = 0.0$  and (b)  $\lambda_f = 0.25$  and  $V_h = 1.0$ .

It should be noted that an inertial sublayer is not easily identified for extremely rough ground surfaces (Cheng et al. 2007). As an example, Fig. 15 compares the vertical profiles of wind speeds in LES against the log-law profile for the cases of  $\lambda_f = 0.25$  with two  $V_h$  values. Based on this graphical procedure, the LES profile fitted with the log-law distribution in the case of  $V_h = 0$  is identified in the height range of  $(1.26\text{--}3.93)h_{av}$ , that is, the depth of  $2.67h_{av}$ . On the other hand, in the case of  $V_h = 1.0$ , the depth of the region fitted with log-law distribution is found to be only  $0.74h_{av}$ . In this way, the depth of the inertial sublayer becomes thinner with a larger  $V_h$  case. As Cheng et al. (2007) described, this fact indicates that the influence of higher buildings on the boundary layer structure is large and the inertial sublayer may not exist for building arrays with highly variable heights, such as extremely rough urban areas. Therefore, the present results also suggest that defining  $z_0$  values becomes more difficult for larger  $\lambda_f$  and  $V_h$  values.

The variations in  $\overline{Cd}$  with  $\lambda_f$  and  $V_h$  are indicated in Fig. 16. In the case of  $V_h = 0.0$ , the change of  $\overline{Cd}$  with  $\lambda_f$  is similar to that seen for the staggered-array case shown in Fig. 11, except for the difference in the  $\overline{Cd}$  value (i.e., a smaller  $\overline{Cd}$  in the square array than in the staggered array). For cases with building height variability, the  $\overline{Cd}$  values significantly increase with the increase in  $V_h$  at each  $\lambda_f$ . When  $\lambda_f \geq 0.50$ , the  $\overline{Cd}$  values become relatively constant at around 1.0.

Xie et al. (2008) performed LESs of turbulent flows over regular arrays of obstacles with random heights and showed that the contributions generated by the tallest obstacles to the total surface drag are the largest among all the obstacles in the computational domain. The results shown in Fig. 16, indicating that the drag coefficient increases with the increase in  $V_h$ , suggest that higher buildings affect the surface drag more significantly; this point, therefore, seems to confirm the results of Xie et al. (2008).

## 6. Predicted aerodynamic roughness parameters over an actual urban area

By applying the results relating  $z_0/h_{av}$  (or  $\overline{Cd}$ ) to the frontal area index and building-height variability as presented in section 5, the aerodynamic roughness parameters for an actual urban area can be estimated from building morphological data like those shown in Table 1. In this section, we calculate the horizontal distribution of the roughness parameters for the central city area of Tokyo. The data presented in section 2 are used for the  $\lambda_f$  and  $V_h$  values.

The  $z_0$  value is calculated by the product of average building height (as shown in Fig. 3b) and normalized roughness length, determined as a function of  $\lambda_f$  and  $V_h$  from the relationship shown in Fig. 14 by linearly interpolating the intermediate values between the data points. For purposes of comparison, the  $z_0$  value is also calculated using a more simplified procedure based only on the frontal area index (i.e., the case with  $V_h = 0$ ). The  $z_0$  distributions over central Tokyo obtained by these two procedures are compared in Fig. 17.

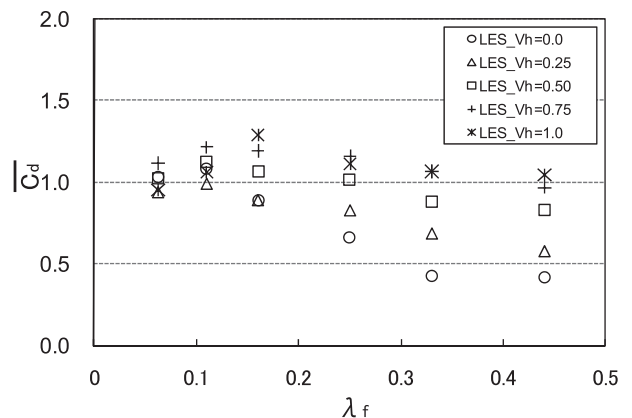


FIG. 16. Variations of  $\overline{Cd}$  with  $\lambda_f$  and  $V_h$  obtained from the present LESs for  $V_h = 0.0, 0.25, 0.50, 0.75$ , and  $1.0$ .

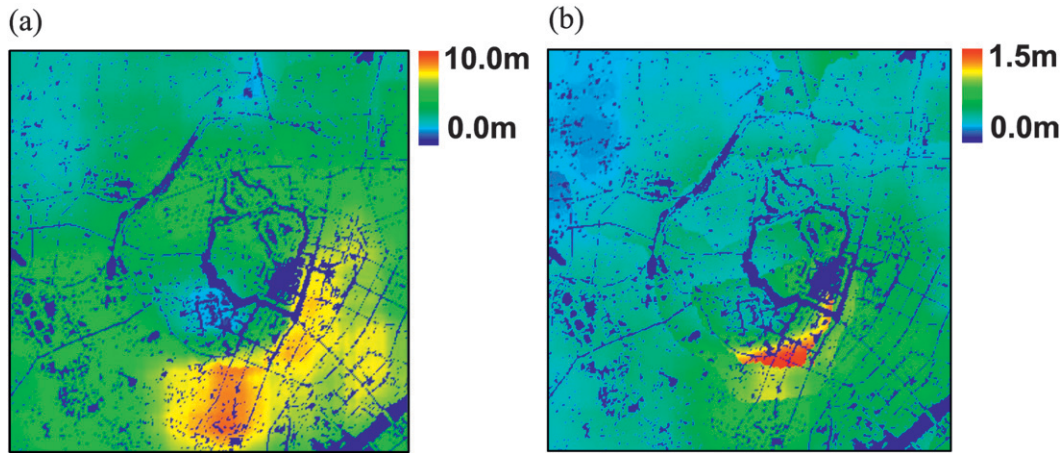


FIG. 17. Spatial distribution of the estimated roughness length  $z_0$  for the area of central Tokyo. The roughness length is assumed to be a function of (a) both  $\lambda_f$  and  $V_h$ , and (b) only  $\lambda_f$ .

From Fig. 17a, the  $z_0$  values are shown to be 5.0–10.0 m in the southern part of the area, where high-rise buildings are densely distributed, and most of the area is characterized by a high roughness of  $z_0 \geq 1.0$  m. On the other hand, Fig. 17b demonstrates that the roughness length is generally lower than or equal to 1.0 m and that high roughness of about 1.5 m is only seen on a localized level in the southern part, where the building packing density is high. Thus, it is important to take into account the variability of building height when estimating the roughness length.

According to the studies by Wieringa (1998) and Grimmond and Oke (1999), the mean values of  $z_0$  over actual urban areas are evaluated as 0.3–2.1 m, with variabilities of less than 1 m. For a city with high-rise buildings and large height variability, like Los Angeles (see Table 1), the roughness length is estimated as high as 14.36 m (Ratti et al. 2002). Since the roughness parameters for Tokyo are similar in magnitude to those of Los Angeles (Table 1), the  $z_0$  values for some areas in Tokyo are expected to exceed 10 m. In this sense, taking building height variability into account when estimating  $z_0$  seems to be appropriate.

Figure 18 shows the spatial distribution of  $\overline{Cd}$  over central Tokyo. The  $\overline{Cd}$  values evaluated as a function of both  $\lambda_f$  and  $V_h$  range between 0.8 and 1.2 in most parts of the Tokyo area (Fig. 18a). In contrast, the  $\overline{Cd}$  values evaluated as a function of only  $\lambda_f$  are about 0.4 in almost all areas of central Tokyo (Fig. 18b). In this way, the value based on the assumption of  $V_h = 0$  is significantly smaller than the estimates with  $V_h \neq 0$ ; this difference is due to the contrasting behavior of  $\overline{Cd}$  in cases between  $V_h = 0$  and  $V_h \neq 0$  for larger  $\lambda_f$  cases (i.e.,  $\lambda_f \geq 0.16$ ; see Fig. 16). In other words, taking the height variability into

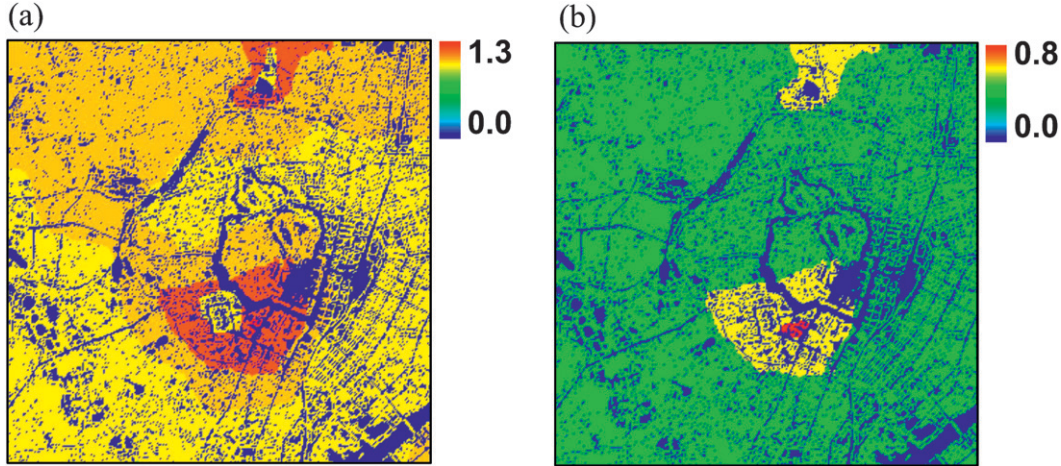
account leads to a horizontal variation in the  $\overline{Cd}$  estimation. According to Brown et al. (2000), the reference values of  $\overline{Cd}$  for urban areas were in the range from 0.7 to 1.5. The present estimates shown in Fig. 18a almost lie within this range.

These estimations made by using building geometrical data such as  $\lambda_f$  and  $V_h$  can also be extended to various types of actual urban areas. Table 3 compares aerodynamic roughness parameters in European and North American cities, as well as in central Tokyo. These roughness parameters were calculated by using the values of  $z_0$  and  $\overline{Cd}$  against  $\lambda_f$  and  $V_h$  according to the relationship shown in Figs. 14 and 16, and the estimates are regarded as area-averaged values. The parameters shown in Table 3 are generally consistent with the observation-based studies of Wieringa (1998), Grimmond and Oke (1998), and Ratti et al. (2002).

The wind-tunnel experiments by Raupach (1992) showed that the drag coefficient value is 0.4 for an array of cubic obstacles. This value is considered to be too small to represent the influence of the actual urban buildings on airflow. Actually, in meteorological simulations of urban boundary layer flows for the Philadelphia metropolitan area performed by using the drag approach, Otte et al. (2004) set the drag coefficient to 1.0 for all urban areas. The results shown in Table 3 suggest that the choice of  $\overline{Cd} = 1.0$  for urban-type areas is reasonable.

## 7. A proposed estimation of aerodynamic roughness for high- $\lambda_f$ cases

As Grimmond and Oke (1999) mentioned, there are two typical approaches to estimating  $z_0$  over urban areas.

FIG. 18. As in Fig. 17, but for  $\overline{Cd}$ .

One is a morphometric method using GIS datasets, and the other is a micrometeorological method using observed data of wind flow based on the logarithmic-profile law. In this study, the latter method was chosen to evaluate both  $z_0$  and  $\overline{Cd}$  depending on  $\lambda_f$  and  $V_h$  from a large number of LESs. However, this method requires a large computational cost for each actual urban area with various roughness properties. Therefore, from a practical point of view, it should still be helpful and desirable to evaluate aerodynamic roughness parameters using the morphometric method.

In this section, we examine the capability for estimating aerodynamic roughness parameters over various surface geometries by applying the theoretical consideration of Macdonald et al. (1998). Their theoretical model computes the value of  $z_0/h_{av}$  from  $\lambda_f$  by assuming that roughness is represented by an array of cubic obstacles. To extend this theoretical consideration to roughness obstacles with variable heights, the following procedure is proposed:

- 1) A building array with variable heights is divided into two groups of building arrays. One is a building array with a height of  $h_{min}$ ; the other a building array with a height of  $(h_{max} - h_{min})$  (Fig. 19a).
- 2) The  $z_0/h_{av}$  values over the arrays of lower buildings with a height of  $h_{min}$  [ $(z_0/h_{av})_{lower}$ ; Fig. 19b] and higher buildings with a height of  $(h_{max} - h_{min})$

[ $(z_0/h_{av})_{higher}$ ; Fig. 19c], are computed by the theoretical equations in Macdonald et al. (1998).

- 3) The  $z_0/h_{av}$  values for each building array computed in the second procedure are combined in proportion to the building height through

$$z_0/h_{av} = [(z_0/h_{av})_{lower} \times h_{min} + (z_0/h_{av})_{higher} \times (h_{max} - h_{min})]/h_{av}. \quad (22)$$

With the use of the above procedure, the  $z_0/h_{av}$  values over building arrays with various combinations of  $\lambda_f$  and  $V_h$  are computed by changing the  $\lambda_f$  value between 0.0625 and 0.44 and the  $V_h$  value between 0.0 and 1.0. The results indicate that the  $z_0/h_{av}$  values increased with  $\lambda_f$  and  $V_h$  (Fig. 20). A comparison of this tendency in Fig. 20 with that in Fig. 14 shows that the present procedure based on the model of Macdonald et al. is quite consistent with the results obtained using LESs. In other words, the proposed procedure can be used for estimating roughness parameters in place of performing LESs. This implies that  $z_0/h_{av}$  values over various geometries of actual urban areas should be diagnosed by the use of the proposed method.

The procedure described above can be further extended to estimate roughness length for flows over urbanlike roughness obstacles with various heights through the incorporation of a multilayer structure in

TABLE 3. Aerodynamic roughness parameters for London, Toulouse, Berlin, Salt Lake City, Los Angeles, and central Tokyo estimated by the relationship obtained from LESs shown in Figs. 13 and 14.

	London	Toulouse	Berlin	Salt Lake City	Los Angeles	Central Tokyo
$z_0$ (m)	0.82	2.5	1.3	2.4	19.5	7.0
$Cd$ (-)	0.69	0.88	0.83	1.21	1.04	1.05

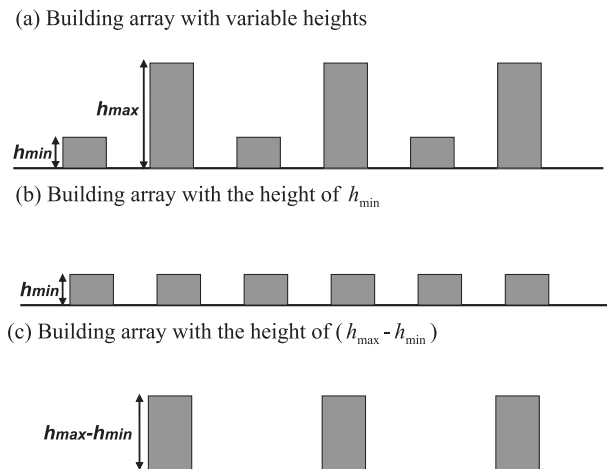


FIG. 19. A schematic of the estimating roughness parameters for building arrays with variable heights: (a) building array with variable heights, (b) building array with the height of  $h_{\min}$ , and (c) building array with the height of  $(h_{\max} - h_{\min})$ .

describing the roughness obstacles, as indicated in Fig. 21. It is first assumed that  $\lambda_f(k)$  is the building frontal area index for a specified height increment  $\Delta h_k$ , and thus  $\lambda_f(k)$  is calculated for each  $\Delta h_k$ . Next, the value of  $z_0/h_{\text{av}}$  at level  $k$  for  $\lambda_f(k)$ ,  $(z_0/h_{\text{av}})_k$ , is calculated by the theoretical model of Macdonald et al. By combining all the values of  $(z_0/h_{\text{av}})_k$  for each  $k$  case (from the ground level to the level of the maximum building height), the value of  $z_0/h_{\text{av}}$  for a complex configuration of the obstacles is obtained. A proposed formulation is expressed as

$$z_0/h_{\text{av}} = \sum_{k=1, N_z} \left[ \frac{z_0}{h_{\text{av}}}(\lambda_f) \right]_k \times \Delta h_k / h_{\text{av}}, \quad (23)$$

where  $N_z$  is the number of levels. This method should be useful in estimating roughness parameters for actual urban areas where the building density and height are highly variable.

## 8. Summary and conclusions

This study investigated the aerodynamic properties of turbulent boundary layer flows over rough surfaces characterized by urbanlike obstacle arrays with various geometries by performing a set of large-eddy simulations (LESs). To set up urbanlike building arrays, we examined building morphological characteristics such as the means and standard deviations of building heights and roughness densities for an area in central Tokyo, and compared them with those for other actual cities. From this analysis, the surface geometries of actual cities were found to demonstrate a wide range not only of

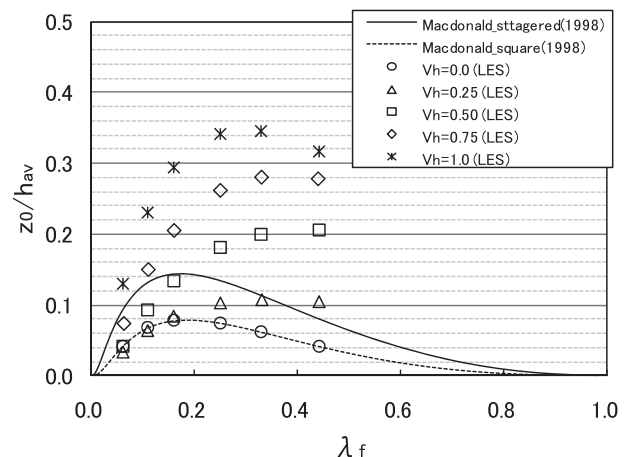


FIG. 20. Variations of  $z_0/h_{\text{av}}$  with  $\lambda_f$  and  $V_h$  by a proposed model.

roughness densities but also of building-height variabilities. This indicated that it is quite difficult to design realistic urban-type surface geometries as regularly arrayed cubical obstacles. Therefore, the urbanlike obstacles set up in the present model have various roughness densities ( $\lambda_f$ ), as well as various height variabilities ( $V_h$ ).

After validating the performance of the LES model developed here, we used the present model to perform a number of sensitivity experiments. The results of the LESs are summarized as follows:

- 1) The roughness lengths normalized by average building heights,  $z_0/h_{\text{av}}$ , in cases of smaller roughness densities ( $\lambda_f \leq 0.16$ ) and smaller height variabilities ( $V_h \leq 0.5$ ), were found to be consistent with the values theoretically derived by Macdonald et al. (1998). For cases with larger roughness densities and height variabilities ( $\lambda_f > 0.16$  and  $V_h > 0.5$ ), the discrepancy in the  $z_0/h_{\text{av}}$  values between the LESs and the theory of Macdonald et al. became more significant with increases in  $\lambda_f$  and  $V_h$ . The values of the drag coefficient,  $\overline{C_d}$ , also increased with the increase in  $V_h$  for a fixed  $\lambda_f$ , while they increased slightly with the increase in  $\lambda_f$  for  $\lambda_f \leq 0.16$  but generally remained unchanged at around 1.0 for higher- $V_h$  cases. For lower- $V_h$  cases, the drag coefficient decreased with the increase in  $\lambda_f$ .

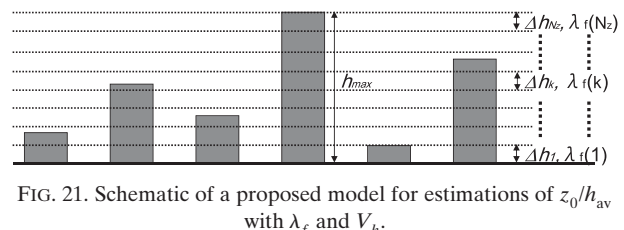


FIG. 21. Schematic of a proposed model for estimations of  $z_0/h_{\text{av}}$  with  $\lambda_f$  and  $V_h$ .

- 2) The aerodynamic roughness parameters for an actual urban area can be evaluated from the relationship between the values of  $z_0$  and  $\overline{Cd}$  with  $\lambda_f$  and  $V_h$  obtained by the LESs. The relationship was applied to an area in central Tokyo, indicating that the roughness length is generally greater than 1.0 m in most of the area and is 5.0–10.0 m in locations where high-rise buildings are densely distributed. The spatial distribution of the  $z_0$  value was more significantly enhanced than that estimated from a relationship as a function of  $\lambda_f$  alone. Furthermore, with variables  $\lambda_f$  and  $V_h$ , the  $Cd$  values ranged between 0.8 and 1.2 in most parts of the area. These values of the aerodynamic roughness parameters were comparable to those in the studies by Wieringa (1998), Grimmond and Oke (1999), and Ratti et al. (2002). On the other hand, when estimating as a function of  $\lambda_f$  alone, both  $z_0$  and  $\overline{Cd}$  were underestimated, particularly for densely built-up areas. These results indicate that it is important to take into account the variability of building height in estimating aerodynamic roughness parameters.

From these LES results, we proposed a method for estimating aerodynamic roughness parameters over various surface geometries by applying and extending the theoretical model of Macdonald et al. (1998), who calculated the value of  $z_0/h_{av}$  from  $\lambda_f$  alone, that is, by assuming that roughness is represented by an array of obstacles with uniform heights. It was found that the method of Macdonald et al. can be extended to an array of building obstacles with various heights by dividing buildings by their heights and applying the formulation of Macdonald et al. for each height range with its corresponding frontal area index. We proposed a formulation to estimate the roughness parameters for actual urban areas that have complex building geometry with multiple height levels and large height variabilities.

In meteorological modeling, the explicit representation of buildings and structures in urban areas is extremely difficult, owing to the geometrical complexity of real cities and the limitations of computational resources. One common approach to dealing with and parameterizing the effects of buildings and structures is to introduce an urban canopy model (as briefly mentioned in section 1). The present study indicates that the roughness properties for realistic urban morphology are characterized more appropriately by taking into account both the densities and heights of roughness obstacles that represent real building configurations. The roughness parameters estimated by the present LESs will be useful in incorporating urban effects in weather forecasting models.

**Acknowledgments.** This study was supported by Grant-in-Aid for Scientific Research 21540453 from the Japan Society for Promotion of Sciences.

## REFERENCES

- Bou-Zeid, E., J. Overney, B. D. Rogers, and M. B. Parlange, 2009: The effects of building representation and clustering in large-eddy simulations of flows in urban canopies. *Bound.-Layer Meteor.*, **132**, 415–436.
- Brown, M. J., 2000: Urban parameterizations for mesoscale meteorological models. *Mesoscale Atmospheric Dispersion*, Z. Boybeyi, Ed., WIT Press, 193–255.
- Cheng, H., and I. P. Castro, 2002: Near wall flow over urban-like roughness. *Bound.-Layer Meteor.*, **104**, 229–259.
- , P. Hayden, A. G. Robins, and I. P. Castro, 2007: Flow over cube arrays of different packing densities. *J. Wind Eng. Ind. Aerodyn.*, **95**, 715–740.
- Chorin, A. J., 1967: A numerical method for solving incompressible viscous flow problems. *J. Comput. Phys.*, **2**, 12–26.
- Coceal, O., T. G. Thomas, I. P. Castro, and S. E. Belcher, 2006: Mean flow and turbulence statistics over groups of urban-like cubical obstacles. *Bound.-Layer Meteor.*, **121**, 491–519.
- Fackrell, J. E., and A. G. Robins, 1982: Concentration fluctuation and fluxes in plumes from point sources in a turbulent boundary layer. *J. Fluid Mech.*, **117**, 1–26.
- Goldstein, D., R. Handler, and L. Sirovich, 1993: Modeling a no-slip flow boundary with an external force field. *J. Comput. Phys.*, **105**, 354–366.
- Grimmond, C. S. B., and T. R. Oke, 1999: Aerodynamic properties of urban areas derived from analysis of surface forms. *J. Appl. Meteor.*, **38**, 1262–1292.
- Hagishima, A., J. Tanimoto, K. Nagayama, and M. Koga, 2009: Aerodynamic parameters of regular arrays of rectangular blocks with various geometries. *Bound.-Layer Meteor.*, **132**, 315–337.
- Hamdi, R., and V. Masson, 2008: Inclusion of a drag approach in the Town Energy Balance (TEB) scheme: Offline 1D evaluation in a street canyon. *J. Appl. Meteor. Climatol.*, **47**, 2627–2644.
- Hiraoka, H., 1993: Modeling of turbulent flows within plant/urban canopies. *J. Wind Eng. Ind. Aerodyn.*, **46/47**, 173–182.
- Jackson, P. S., 1981: On the displacement height in the logarithmic profile. *J. Fluid Mech.*, **285**, 69–94.
- Jimenez, J., 2004: Turbulent flows over rough walls. *Annu. Rev. Fluid Mech.*, **36**, 173–196.
- Kanda, M., 2006: Large-eddy simulations on the effects of surface geometry of building arrays on turbulent organized structures. *Bound.-Layer Meteor.*, **118**, 151–168.
- Macdonald, R. W., R. F. Griffiths, and D. J. Hall, 1998: An improved method for the estimation of surface roughness of obstacle arrays. *Atmos. Environ.*, **32**, 1857–1864.
- Martilli, A., and J. L. Santiago, 2007: CFD simulation of airflow over a regular array of cubes. Part II: Analysis of spatial average properties. *Bound.-Layer Meteor.*, **122**, 635–654.
- , A. Clappier, and M. W. Rotach, 2002: An urban surface exchange parameterization for mesoscale models. *Bound.-Layer Meteor.*, **104**, 261–304.
- Maruyama, T., 1993: Optimization of roughness parameters for staggered arrayed cubic blocks using experimental data. *J. Wind Eng. Ind. Aerodyn.*, **46/47**, 165–171.

- Masson, V., 2006: Urban surface modeling and the meso-scale impact of cities. *Theor. Appl. Climatol.*, **84**, 35–45.
- , and Y. Seity, 2009: Including atmospheric layers in vegetation and urban offline surface schemes. *J. Appl. Meteor. Climatol.*, **48**, 1377–1397.
- Otte, T. L., A. Lacser, S. Dupont, and J. K. S. Ching, 2004: Implementation of an urban canopy parameterization in a mesoscale meteorological model. *J. Appl. Meteor.*, **43**, 1648–1665.
- Ratti, C., S. Di Sabatino, R. Britter, M. Brown, F. Caton, and S. Burian, 2002: Analysis of 3-D urban databases with respect to pollution dispersion for a number of European and American cities. *Water Air Soil Pollut. Focus*, **2**, 459–469.
- Raupach, M. R., 1992: Drag and drag partition on rough surfaces. *Bound.-Layer Meteor.*, **60**, 375–395.
- Santiago, J. L., Coceal, O., Martilli, A., and Belcher, S. E., 2008: Variation of the sectional drag coefficient of a group of buildings with packing density. *Bound.-Layer Meteor.*, **128**, 445–457.
- Smagorinsky, J., 1963: General circulation experiments with the primitive equations. *Mon. Wea. Rev.*, **91**, 99–164.
- Sorbian, Z., and M. Uliasz, 1982: Some numerical urban boundary-layer studies. *Bound.-Layer Meteor.*, **22**, 481–502.
- Tseng, Y. H., C. Meneveau, and M. B. Parlange, 2006: Modeling flow around bluff bodies and predicting urban dispersion using large eddy simulation. *Environ. Sci. Technol.*, **40**, 2653–2662.
- Van Driest, E. R., 1956: On turbulent flow near a wall. *J. Aerosp. Sci.*, **23**, 1007–1011.
- Wieringa, J., 1998: Representative roughness parameters for homogeneous terrain. *Bound.-Layer Meteor.*, **63**, 323–363.
- Xie, Z. T., and I. P. Castro, 2006: LES and RANS for turbulent flow over arrays of wall-mounted obstacles. *Flow Turbul. Combust.*, **76**, 291–312.
- , O. Coceal, and I. P. Castro, 2008: Large-eddy simulation of flows over random urban-like obstacles. *Bound.-Layer Meteor.*, **129**, 1–23.